The EMBO Journal vol.13 no.5 pp.1011 - 1018, 1994

# Three-dimensional structure of the rotavirus haemagglutinin VP4 by cryo-electron microscopy and difference map analysis

**Mark Yeager[1], John A.Berriman[2], Timothy S.Baker[3] and A.Richard Bellamy[4]**

The Scripps Research Institute, Departments of Cell and Molecular Biology, MB6, 10666 North Torrey Pines Road, La Jolla, CA 92037, [3]Department of Biological Sciences, Purdue University, West Lafayette, IN 47907-1392, USA, [2]MRC Laboratory of Molecular Biology, Hills Road, Cambridge, UK and [4]Biochemistry and Molecular Biology, School of Biological Sciences, University of Auckland, Auckland, New Zealand

[1]Corresponding author

Footnote: Presented in part at the 1992 joint meeting of the ASBMB and the Biophysical Society.

Communicated by N.Unwin

**The three-dimensional structure of the rotavirus spike haemagglutinin viral protein 4 (VP4) has been determined to a resolution of 26 Å by cryo-electron microscopy and difference analysis of intact virions and smooth (spikeless) particles. Native and spikeless virions were mixed prior to cryo-preservation so that both structures could be determined from the same micrograph, thereby minimizing systematic errors. This mixing strategy was crucial for difference map analysis since VP4 only accounts for ~1% of the virion mass. The VP4 spike is multi-domained and has a radial length of ~200 Å with ~110 Å projecting from the surface of the virus. Interactions between VP4 and cell surface receptors are facilitated by the bi-lobed head, which allows multi-site interactions, as well as the uniform distribution of the VP4 heads at maximum radius. The bi-lobed head is attached to a square-shaped body formed by two rods that have a slight left-handed helical twist. These rods merge with an angled, rod-like domain connected to a globular base ~85 Å in diameter. The anchoring base displays pseudo 6-fold symmetry. This surprising finding may represent a novel folding motif in which a single polypeptide of VP4 contributes similar but non-equivalent domains to form the arms of the hexameric base. The VP4 spike penetrates the virion surface ~90 Å and interacts with both outer (VP7) and inner (VP6) capsid proteins. The extensive VP4-VP7 and VP4-VP6 interactions imply a scaffolding function in which VP4 may participate in maintaining precise geometric register between the inner and outer capsids. Finally, we hypothesize that the close interactions between VP4 and VP6 may allow binding of VP4 to immature inner capsid particles in the viroplasm, which then bud through the membrane of the ER to acquire the outer capsid layer that is formed by VP7.**

*Key words*: cryo-electron microscopy/image processing/ haemagglutinin/rotavirus

## Introduction

Rotavirus is the major cause of infant mortality in developing countries by causing severe gastroenteritis (Kapikian and Chanock, 1990). Cryo-electron microscopy is a powerful method for determining the low resolution structure of such large viruses (diameter ~1000 Å), which to date have not been amenable to high resolution X-ray crystallography. The native three-dimensional structure of these large particles can be derived by preserving unstained specimens in the frozen-hydrated state (Adrian *et al.*, 1984; Unwin, 1986; Dubochet *et al.*, 1988). Since the specimens are unstained, image processing helps delineate internal as well as external features.

Cryo-electron microscopy and icosahedral image reconstruction techniques have previously been used to examine the native three-dimensional structure of rhesus rotavirus (Yeager *et al.*, 1990). The density maps revealed that the outer and inner capsids display $T = 13\,l$ icosahedral lattice symmetry, are centered at radii of 377 Å and 299 Å, respectively, and are perforated by 40-65 Å diameter holes which are in radial register between the outer and inner capsids. In addition, a third protein layer, centered at a radius of 255 Å, encapsidates the double stranded RNA genome. This triple-layered organization of rhesus rotavirus was clearly revealed in radial density plots (Yeager *et al.*, 1990) and was recently confirmed by Shaw *et al.* (1993) for strain SA11.

A striking feature of the density maps is the presence of 60 spikes that project from the outer capsid surface. By Fab labeling (Prasad *et al.*, 1990) and biochemical analysis (Anthony *et al.*, 1991) the spikes have been identified as viral protein 4 (VP4), an 88 kDa outer capsid protein that serves as the viral haemagglutinin (Kalica *et al.*, 1983), as a neutralization antigen (Mackow *et al.*, 1988b) and as a determinant of virulence (Flores *et al.*, 1986; Gorziglia *et al.*, 1986; Offit *et al.*, 1986). In the presence of trypsin, VP4 is cleaved to VP5* (60 kDa) and VP8* (28 kDa) which confers infectivity (Graham and Estes, 1980; Clark *et al.*, 1981; López *et al.*, 1985, 1986) and allows virions to penetrate intestinal epithelial cells (Fukuhara *et al.*, 1987; Kaljot *et al.*, 1988).

Biochemical analysis indicates that alkali treatment causes specific release of VP4, generating spikeless virions (Anthony *et al.*, 1991). We have separately purified and mixed native and spikeless (i.e. lacking VP4) virions of rotavirus strain SA11 to form a single sample for cryo-electron microscopy. This approach provided an essential control of experimental variables for attempting difference map analysis since VP4 only accounts for ~1% of the virion mass (Liu *et al.*, 1988). Variations in magnification, defocus, optical density and ice thickness were minimized by collecting both data sets from one image. This approach enabled the determination of the overall three-dimensional structure of VP4 in its native state and its interactions with

outer and inner capsid proteins. Combining the mixing strategy and difference map analysis is an electron microscopic application of isomorphous replacement, except that the examined moiety (i.e. VP4) has been removed in our case. This is equivalent to the determination of the structure of a prosthetic group by comparing the native and apo forms of a protein.

Our preliminary analysis of the VP4 structure was at 35 Å resolution (Yeager *et al.*, 1992), and we report here our analysis at 26 Å resolution. An analysis of reassortant forms of rotavirus using cryo-electron microscopy and image processing has recently appeared (Shaw *et al.*, 1993). One of the reassortant viruses displayed diminished infectivity after purification, attributed to a reduction in the number of VP4 spikes per particle. A difference map between virions with spikes and the reassortant with reduced occupancy at the VP4 sites allowed the determination of a structure for VP4. Although completely different strategies were used for our study, the conclusions reached about the general dimensions and asymmetric, multi-domained structure of VP4 are similar. However, the VP4 map presented here displays better definition of the domains and external

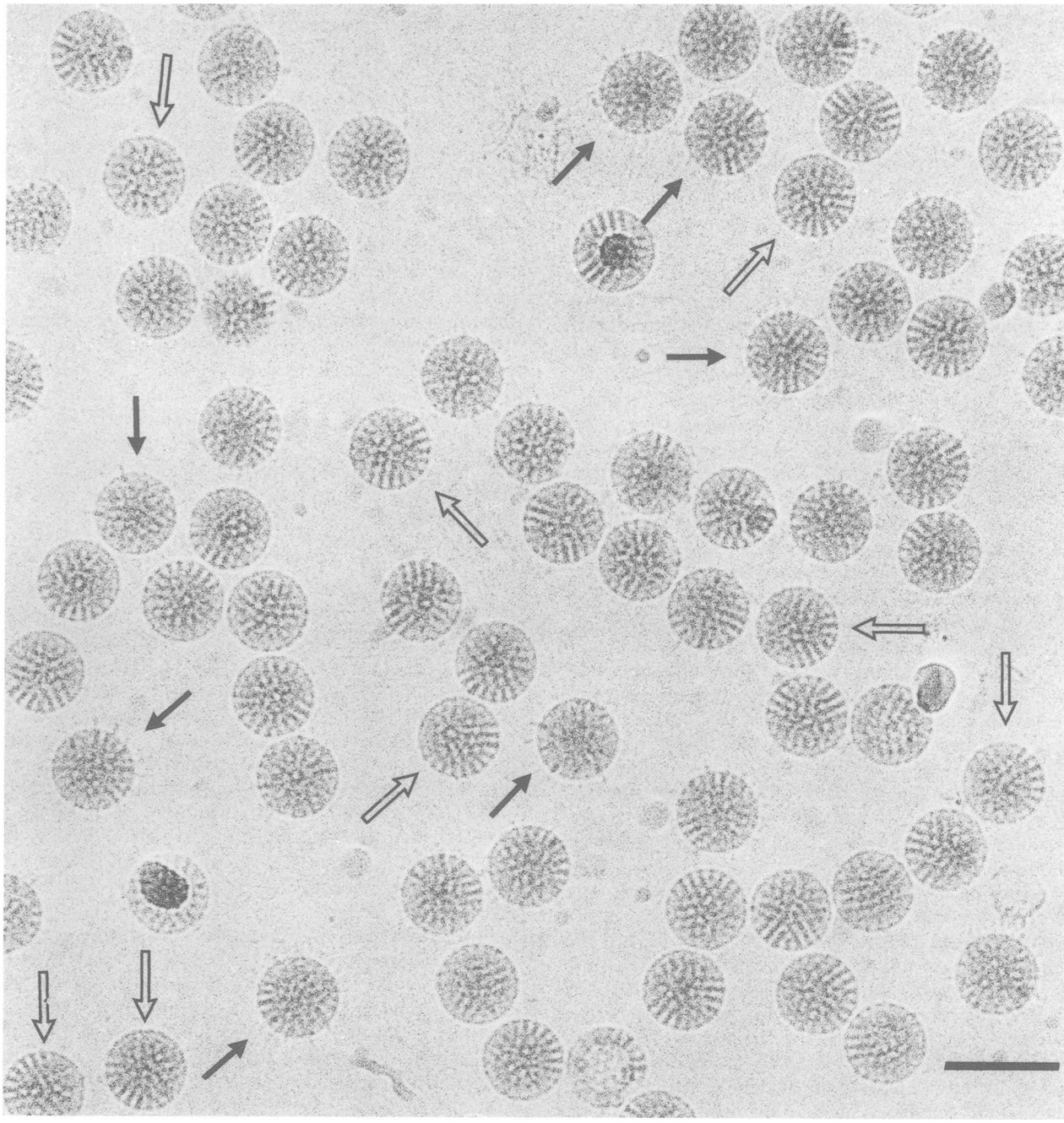

**Fig. 1.** Image of unstained, frozen–hydrated SA11 rotavirus sample. Native virions with intact VP4 spikes (solid arrows) and virions that lack VP4 due to alkali treatment (open arrows) were separately purified and then mixed prior to cryo-preservation. Native and spikeless virions are readily distinguished in this micrograph recorded at ~3 μm defocus. Mixing the two samples helps minimize systematic errors due to variations in magnification, defocus, and optical density, thereby enabling the calculation of a difference map between the native and spikeless virions to derive the three-dimensional map of VP4. Scale bar = 1000 Å.

contours of VP4, probably because (i) the native and spikeless particles were mixed and photographed in the same field, (ii) alkali treatment quantitatively releases all spikes from the virions (Anthony *et al.*, 1991) so that the occupancy at the VP4 sites in the spikeless particles is effectively zero, and (iii) more particles were used in our analysis so the data extend to higher resolution. Our difference map displayed very little noise and revealed that the VP4 spike is formed by a dimeric head attached to a base with pseudo 6-fold symmetry. This surprising finding may indicate the presence of a novel folding motif in which a single polypeptide of VP4 contributes similar but non-equivalent domains in forming the arms of the hexameric base.

## Results

### *Cryo-electron microscopy and image reconstruction*

Image pairs were recorded from selected fields, first at 0.8 μm and then at 3 μm defocus. The second, strongly defocussed image readily allowed the virions with and without the spikes to be distinguished (Figure 1). The companion micrograph, recorded at 0.8 μm defocus, was used for image processing since it displayed a contrast transfer function which was of constant sign to ~20 Å resolution. The derived particle orientations were uniformly distributed over the icosahedral asymmetric unit (Figure 2a) ($\theta$ = 69–90°; $\varphi$ = −32–32°; $\omega$ = 0–180°) thereby allowing reliable interpolation of the three-dimensional Fourier transform. Cross-correlation analysis of the native and spikeless maps (Figure 2b) indicated that the resolution limit was ~26 Å, based on a cut-off value of 0.5. This resolution value is conservative since the final maps were computed from twice as many particles as used for the cross-correlation analysis. It is noteworthy that the profile comparing the native and spikeless maps (Figure 2b) displays reduced correlation at low resolution (~1/90 Å$^{-1}$) and higher correlation at higher resolution. VP4 presumably causes a low resolution perturbation in the correlation profile due to its distribution over the surface of the particle. The improved correlation at higher resolution indicates that VP4 in fact contributes very little to the overall density in the map, consistent with the fact that VP4 accounts for only ~1% of the mass of the virion.

### *Biochemical and structural integrity of spikeless rotavirus*

The three-dimensional density map of spikeless rotavirus (Figure 3b) shows striking similarity to native SA11 rotavirus (Figure 3a) in icosahedral symmetry, in the number and distribution of surface holes, as well as in the rippled outer capsid surface. The outer and inner capsids both display $T$ = 13 $l$ icosahedral symmetry, and radial density maps (data not shown) show no change in the overall distributions of mass density in the three protein layers following alkali treatment. SDS gel electrophoresis profiles (Anthony *et al.*, 1991) show that VP4 is selectively released after alkali treatment with complete retention of the other structural proteins in the spikeless virions. Integrity of the protein structure was also indicated by recognition of alkali-treated virions by a monoclonal antibody directed against VP7, the major outer capsid protein (Anthony *et al.*, 1991).

Any loss of mass due to release of RNA after alkali treatment could potentially complicate the interpretation of difference maps. In order to examine the effect of alkali treatment on the viral RNA, virions with $^{32}$P-labeled RNA were prepared. In two separate experiments, 95–97% of the radioactivity in $^{32}$P-labeled RNA was retained by both the native and alkali-treated virions. Therefore, virtually no viral RNA is released from the virions as a consequence of alkali treatment. However, gel electrophoresis (data not shown) revealed that alkali treatment introduced single strand breaks in the dsRNA genome and that the RNA was degraded to fragments ~200–500 bp in length.

### *Comparison of the structures of strains SA11 and rhesus rotavirus*

The three-dimensional density map of native SA11 rotavirus (Figure 3a) displays a surface with $T$ = 13 $l$ icosahedral lattice symmetry comparable with rhesus rotavirus (Yeager *et al.*, 1990) and with that of a recent determination of SA11 rotavirus (Shaw *et al.*, 1993). The 132 holes in the rippled outer capsid surface (Figure 3a) are closely comparable with the structure of rhesus rotavirus. In addition, radial density maps (data not shown) reveal a three-layered capsid organization with prominent density peaks at radii nearly identical to those observed in rhesus rotavirus (Yeager *et al.*, 1990). The map of SA11 rotavirus at 26 Å resolution (Figure 3a) displays the same complex morphology of the VP4 spikes as found in the map of rhesus rotavirus (Yeager

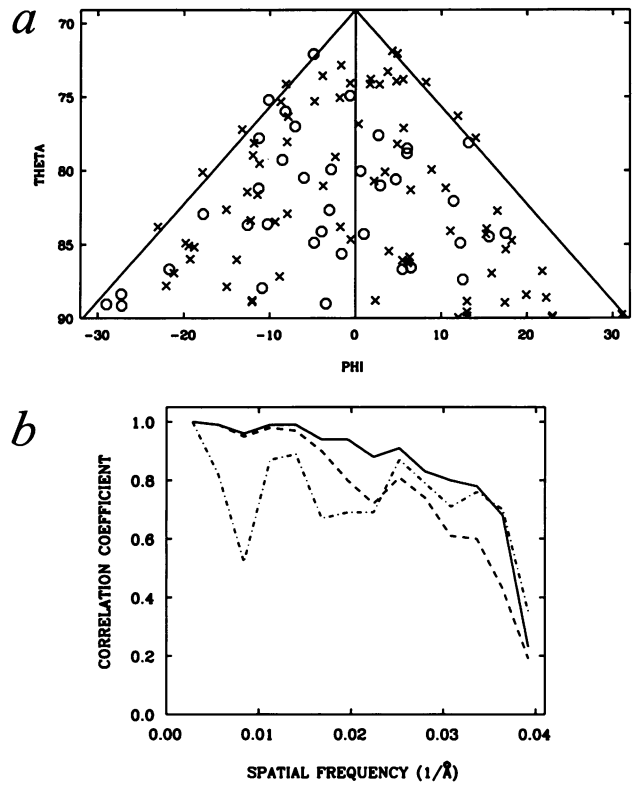


**Fig. 2.** (**a**) Plot of the refined $\theta$,$\phi$ orientation angles for the native (o) and spikeless (x) SA11 rotavirus images derived from the particles displayed in Figure 1. The plot demonstrates that the data encompass a uniform distribution of orientations so that a reliable three-dimensional reconstruction can be computed. (**b**) Cross-correlation analysis. The native and spikeless particle image data sets were randomly divided, and two independent reconstructions were computed for the native (– – – –) and spikeless (——) virions. The maps were compared pairwise versus spatial frequency as indicated. The native and spikeless maps (– · – · –) were also compared in a similar fashion. Perfectly matched data would have a correlation coefficient of 1, and random data would have a coefficient of 0.

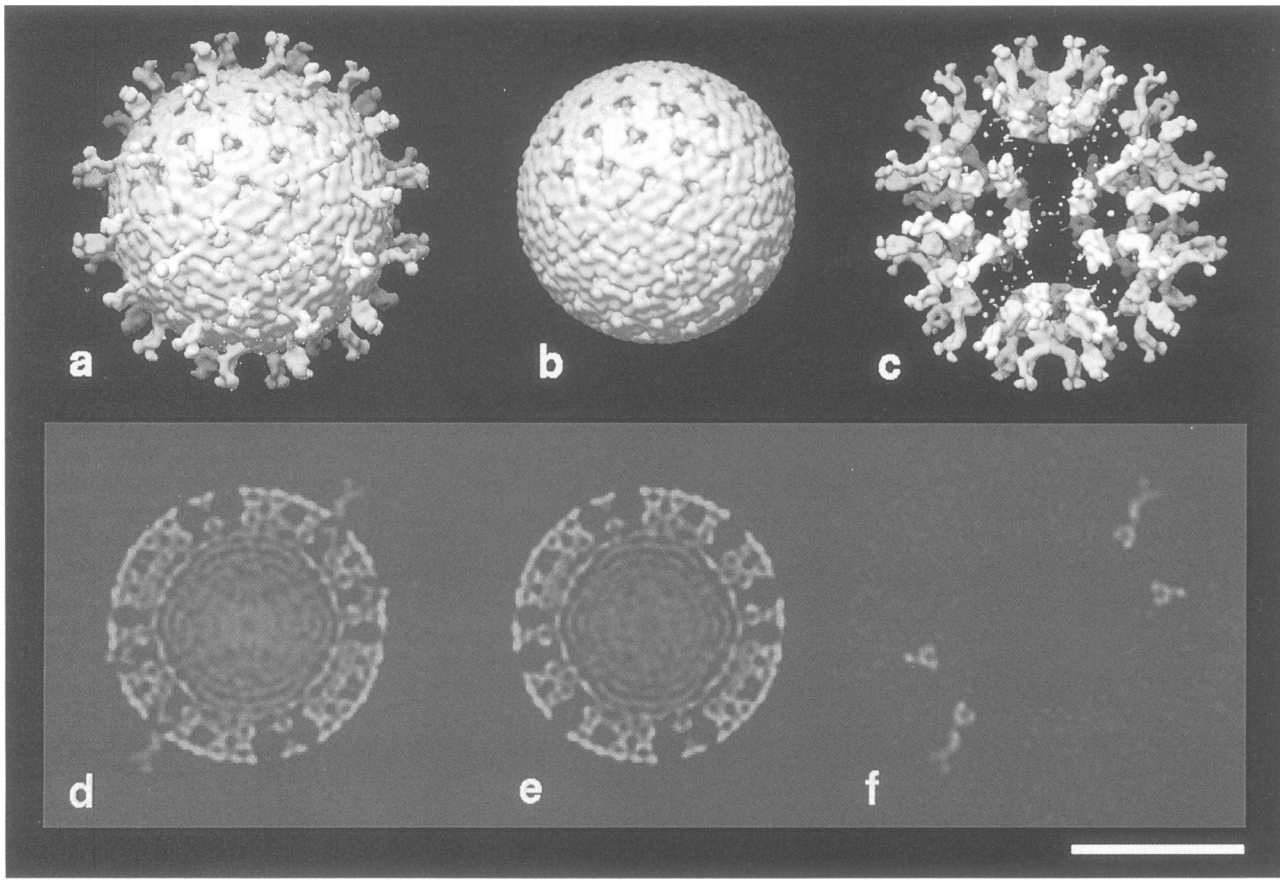


**Fig. 3.** Surface-shaded representations of the native SA11 rotavirus (**a**), spikeless rotavirus (**b**), and the difference map (**c**), viewed down an icosahedral two-fold symmetry axis. Shown in (**d**), (**e**) and (**f**) are planar sections (~14 Å thick) from the corresponding native, spikeless, and difference maps which reveal the characteristic structural features of the spike. The image processing procedures enforce icosahedral symmetry on the RNA; therefore, density at radii corresponding to the location of the RNA has been set to the background value in the difference map. To compute the difference map (c), the native and spikeless maps were scaled to give a maximum correlation of the corresponding density values that lie between radii of ~205 Å and 360 Å, thereby correcting for the different numbers of particles used for computing the two maps. Scale bar = 500 Å.

*et al.*, 1990) and SA11 rotavirus (Yeager *et al.*, 1992) at 35 Å resolution. The orientation of the bi-lobed head is in the same orientation with respect to the icosahedral surface lattice. Therefore, there appears to be overall conservation in the geometry and orientation of the VP4 haemagglutinin between strains SA11 and rhesus rotavirus. Previous maps of SA11 rotavirus at 40 Å resolution (Prasad *et al.*, 1988) and 35 Å resolution (Prasad *et al.*, 1990) did not show such clear definition of the bi-lobed head as in Figure 3. The conservation in globular folding is consistent with the high degree of homology (~85%) between the amino acid sequences of different rotavirus strains (López *et al.*, 1985; López and Arias, 1987; Mackow *et al.*, 1988b; Nishikawa *et al.*, 1988; Mitchell and Both, 1989).

## Discussion

We previously noted the disparity between the stoichiometry of VP4 based on icosahedral symmetry and full occupancy of all 60 sites (Yeager *et al.*, 1990) and that determined by biochemical analysis (Liu *et al.*, 1988). In fact, volume calculations suggested that only a portion of VP4 might be exposed at the outer capsid surface, with the remainder embedded within the interior of the virion. Since the native and spikeless virions are structurally isomorphous, this possibility was investigated by calculating a difference density map between the native and spikeless virions (Figure 3c), described below.

### *Three-dimensional structure of the VP4 haemagglutinin*

A difference density map between the native (Figure 3a) and spikeless (Figure 3b) virions reveals the complex shape and multi-domain organization of the VP4 spike (Figures 3c and 4). The bi-lobed globular heads have axes measuring 28–32 and 40–42 Å and appear to narrow at their site of connection to a roughly square-shaped body (~25 Å thick, ~65 Å high and 50–60 Å wide). This body appears to be formed by two rods of density (~25 Å diameter and ~65 Å long) that have a slight left-handed helical twist with respect to each other. These radially oriented rods coalesce and attach to a single, wider rod-like domain (~32 Å diameter and ~75 Å long) that is sharply angled by ~120°. This angled rod of density is attached at its proximal end to a globular base (~85 Å diameter). This base or pedestal appears to display 6-fold symmetry when viewed from the bottom (Figure 4, bottom right) with a central depression which can be resolved as a 'channel' ~40 Å in length when viewed in cross-section (Figure 5a). The functional significance of this 'channel' is unclear at this time.

The elongated shape of VP4 with multiple domains resembles the haemagglutinin of influenza virus (Wilson *et*

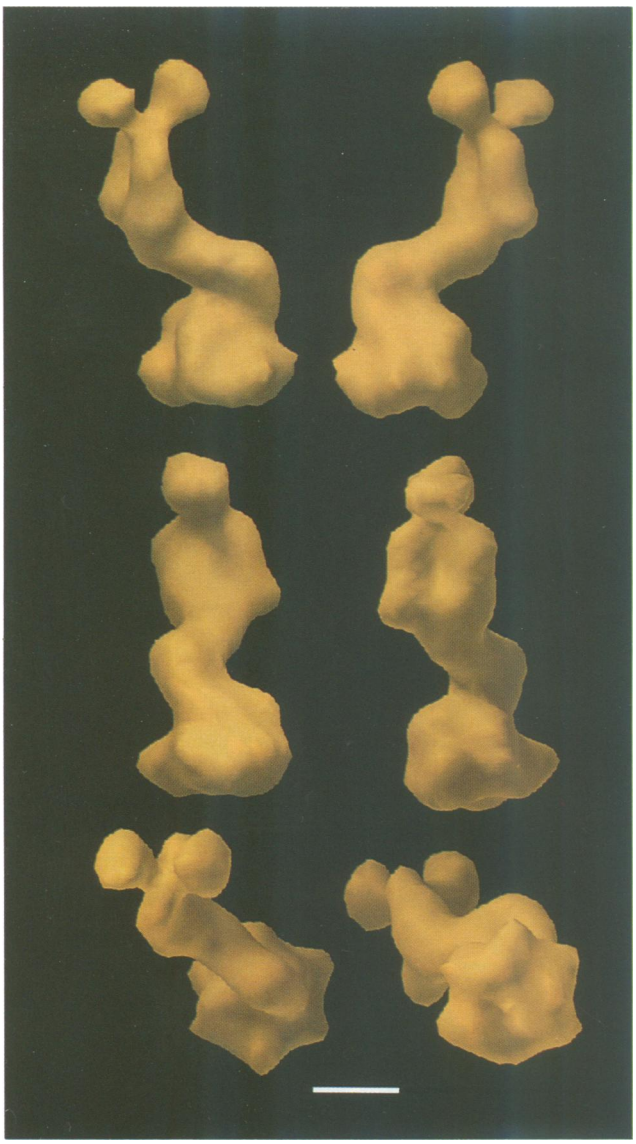

**Fig. 4.** Montage of magnified views of the rotavirus VP4 haemagglutinin. The top and middle panels display four distinct side views and the bottom panel displays glancing views of the top and bottom, respectively, shown at the left and right. Scale bar = 50 Å.

*al.*, 1981), which is a trimeric membrane protein with distinct rod-like and globular regions. However, the stoichiometry of the VP4 spikes appears to favor a dimer based on the bi-lobed head and dimeric body (Figure 4), interaction with two Fab fragments (Prasad *et al.*, 1990) and stoichiometry based on *in vivo* radiolabeling (Shaw *et al.*, 1993). The rod-like portion of the influenza haemagglutinin forms a triple-stranded, coiled-coil of α-helices. Interestingly, secondary structure predictions for VP4 suggest that the molecule may contain extended α-helical regions packed as coiled-coils (López *et al.*, 1991). Higher resolution analysis will be required to discern whether the rod-like domains of VP4 are folded as α-helices.

The surprisingly noise-free difference map (Figure 3c and f) only displays significant density corresponding to the VP4 spike. The globular base of VP4 penetrates to radii corresponding to the inner capsid surface (violet in Figure 5) that is formed by pillar-shaped trimers of VP6, a 45 kDa protein that serves as the sub-group specific antigen (Martin *et al.*, 1975; Esparza and Gill, 1978; Gorziglia *et al.*, 1985). If there were protein rearrangements of VP6 and/or VP7 during the alkali treatment to release VP4, then the difference map would display both positive and negative peaks, but only positive density is seen. Therefore, the native and spikeless particles are indeed isomorphous, and the globular base is a bonafide feature. Although we cannot absolutely rule out that another structural protein(s) forms the base, there is no biochemical evidence that the material released after alkali treatment contains a significant amount of non-VP4 polypeptides. It therefore appears that the VP4 spike has an intriguing organization of domains with a bi-lobed head and an anchoring base with pseudo 6-fold symmetry. If the spike is a VP4 dimer, then each head corresponds to a monomer, but it is not clear how a single polypeptide forms half of each base. For instance, each polypeptide could form three domains at the base which contribute three arms of the hexamer. Another possible organization for VP4 is that a single polypeptide could give rise to six domains with pseudo 6-fold symmetry, and both polypeptides in the dimer would contribute to each arm of the hexamer. Even though we cannot define the folding of the polypeptide within the base, the dimeric spike attached to a hexameric base suggests that similar but non-equivalent domains of VP4 interact with different VP6 molecules. It is notable that the binding of VP4 to the six VP6 trimers is not random since the VP4 molecules have a precise orientation with respect to the 5-fold symmetry axis. If the binding interactions between VP4 and VP6 were equivalent, then one would expect that the six possible orientations for VP4 would smear the density in the map. The precise orientation for binding of the VP4 spikes is presumably dictated by the non-equivalent interactions between VP4 and VP6 as well as by the unique interactions between VP4 and VP7 at the edge of the Type II hole (see below). Delineation of the precise interactions between VP4 with VP6 and VP4 with VP7 requires an analysis at higher resolution.

### *Interactions of VP4 with rotavirus proteins*

Previous analysis of rhesus rotavirus (Yeager *et al.*, 1990) revealed that the VP4 spike is attached to the virion surface at the edge of the Type II hole (i.e. the holes on the local 6-fold symmetry axes closest to the 5-fold axes) in contact with VP7, a 34 kDa glycoprotein that induces serotype specific neutralization antibodies (Kalica *et al.*, 1981; Mackow *et al.*, 1988a) (blue in Figure 5). However, it was not clear whether VP4 had any other sites of attachment or interactions beneath the virion surface. The difference map (Figure 3c) clearly reveals that VP4 has an asymmetric, elongated structure that spans radii from ~300 to 500 Å. As previously determined, the three protein layers are centered at radii of 255, 299, and 377 Å. VP4 therefore clearly extends well below the virus surface to radii that allow extensive interactions with the two capsid layers. For example, comparison of selected planar sections in the native and spikeless density maps (Figure 3d, e and f) reveals that the VP4 spikes project from the outer capsid surface and penetrate deeply into the Type II hole.

Surface-shaded renderings that combine the VP4 spike map (Figure 3c) and the spikeless virion map (Figure 3b) allow closer examination of the interactions between VP4 and other rotavirus proteins (Figure 5). VP4 makes close contact with VP7 (blue in Figure 5) throughout the outer

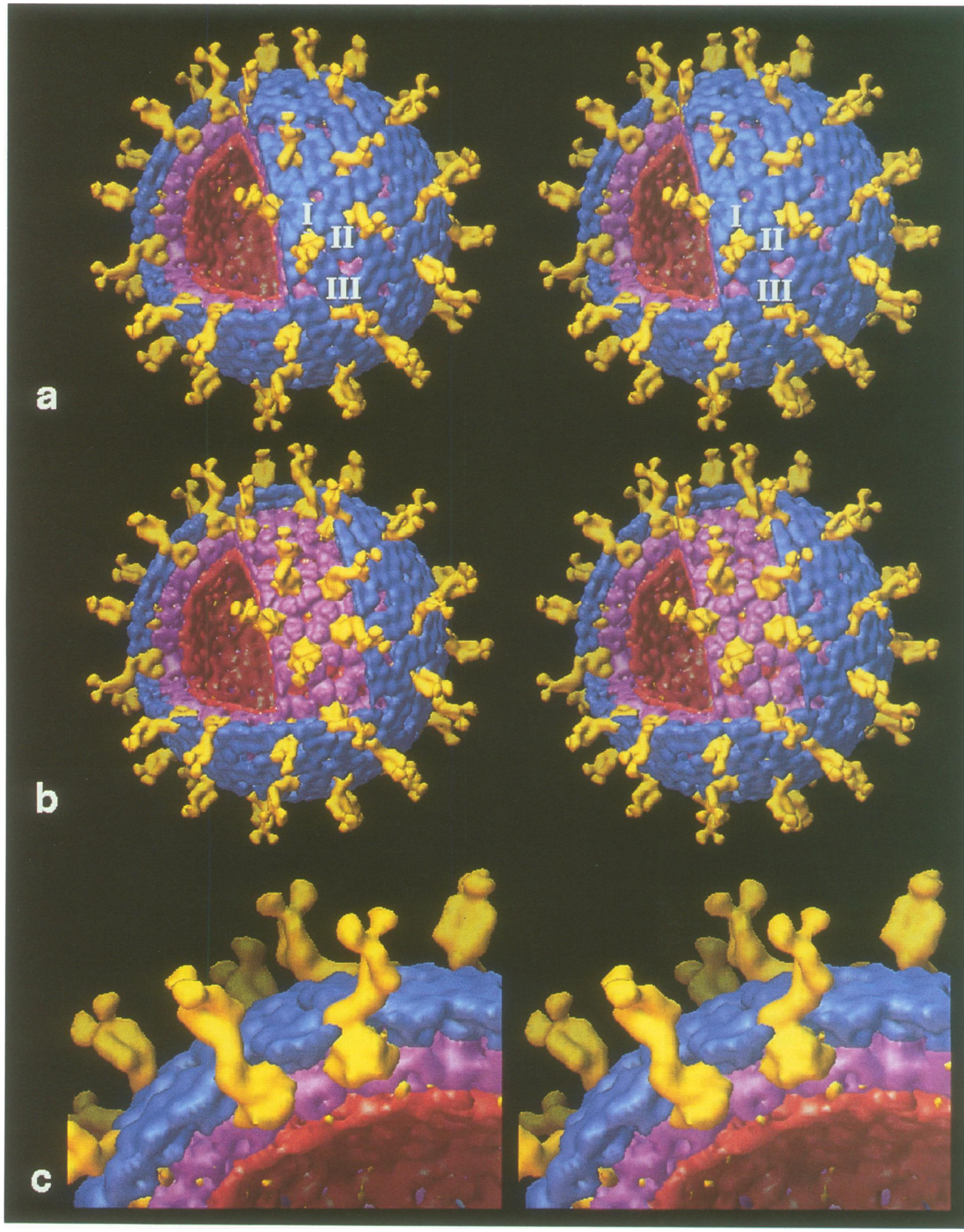


**Fig. 5.** The three-dimensional surface-shaded stereo representations viewed towards the 5-fold symmetry axis display the VP4 spikes (yellow), which have a radial length of ~200 Å, and the three protein shells of rotavirus: blue = outer capsid shell formed by VP7; violet = inner capsid shell formed by VP6; and red = core shell formed primarily by VP2, as well as VP1 and VP3. The radii for approximately defining the three protein layers are based on the mass distribution in a radial density plot (Yeager *et al.*, 1990). The outer capsid is perforated by 132 holes of three types [identified by labels in (**a**)]: 12 Type I holes at the icosahedral vertices; 60 Type II holes at the peripentonal positions; and 60 Type III holes encircling the icosahedral 3-fold axes of symmetry. The 60 VP4 spikes reside within the Type II peripentonal holes. (a) View of the outer capsid surface reveals interactions between VP4 and VP7. (**b**) The outer capsid layer has been partially removed to reveal the interactions between VP4 and VP6 in the inner capsid. (**c**). Close-up view showing the side-to-side interactions between VP4 and the outer and inner capsids.

capsid layer (Figure 5a and c). In addition, VP4 interacts with the VP6 trimers in the inner capsid (Figure 5b and c). The density in the difference map is at the noise level in regions corresponding to the maximum density in the inner capsid and the core layer (red in Figure 5) thought to be formed primarily by VP2, as well as VP1 and VP3 (Bican *et al.*, 1982; Liu *et al.*, 1988; Labbé *et al.*, 1991). The portion of VP4 closest to the outer capsid surface corresponds to the angled, rod-like portion of VP4 that connects the body to the anchoring base. This rod-like domain of VP4 makes extensive contact with VP7 (blue in Figure 5) along the edge of the Type II, peripentonal hole (compare Figure 3a and b; Figure 5). The distal end of the rod is located above and off to one side (opposite the 5-fold axis) of the Type II hole, and the proximal end resides just inside the Type II hole on the side which is closest to the Type I (5-fold) hole. The proximal end of the rod merges with VP4 density which radially penetrates the outer capsid and forms the hexameric base or pedestal of VP4. The VP4 base resides at radii within the inner capsid layer (violet in Figure 5), near the axes of strict, 5-fold symmetry, allowing bonding only at the VP6 trimer positions that are equivalent. Each hexameric VP4 base interdigitates between hexameric clusters of VP6 trimers, and these close interactions may help stabilize the inner capsid layer.

### *Functional implications*

In addition to serving as a ligand for cell surface receptors, as a haemagglutinin and as a neutralization antigen, this analysis suggests two additional features of VP4 that may have functional importance. First, the extensive VP4–VP7 and VP4–VP6 interactions suggest a possible scaffolding function in which VP4 may participate in maintaining precise geometric register between the inner and outer capsids. Secondly, VP4 is extremely well designed to maximize interactions with cell surface receptors. The bi-lobed head allows multi-site interactions with receptors. Also, the angled rod domain of VP4 that connects the base and body shifts the bi-lobed heads away from the 5-fold symmetry axes. This splaying apart of the heads provides a more uniform distribution over the virion surface compared with the anchoring bases that are clustered around the 5-fold axes (Figures 3c and 5a) and therefore may increase the probability of VP4 binding to cell surface receptors. As noted above, the conformational changes induced by trypsin cleavage of VP4 render the virus infective. It will now be important to delineate the extent to which trypsin induces conformational changes in VP4 and how these might affect virion structure.

### *Implications for virus assembly*

Early in the morphogenesis of rotavirus, an immature particle (the 'single-shelled particle'), which contains the core formed by VP1, VP2 and VP3 and the inner capsid layer formed by VP6, undergoes self-assembly within the cytoplasm of the infected cell. This particle then buds into the lumen of the endoplasmic reticulum (Bellamy and Both, 1990). This process is initiated by the interaction of the immature particle with the NS28 receptor. This viral, non-structural membrane glycoprotein is localized in the endoplasmic reticulum of the infected cell. After budding, the particle becomes transiently enveloped in a membrane vesicle, the outer capsid proteins VP7 and VP4 are assembled onto the particle, and the membrane is then removed (Poruchynsky and Atkinson, 1985). Assembly of the outer capsid proteins imposes a requirement that they both be available in the vesicle or the lumen of the endoplasmic reticulum where the immature particle is located. VP7 is an integral membrane protein and is translocated completely into the lumen (Kabcenell and Atkinson, 1985; Stirzaker *et al.*, 1987). However, it is not known how VP4, which lacks a hydrophobic leader sequence (Bellamy and Both, 1990), crosses the membrane. Based on our results, it is possible that the VP4 spikes may first bind to the immature particle in the cytoplasm via interactions with VP6. VP7 may then be added as the particle with bound VP4 buds through the endoplasmic reticulum. Experiments that examine the binding of VP4 to single-shelled particles and to spikeless virions should allow this hypothesis to be tested.

### *Conclusions*

The three-dimensional structure of the rotavirus spike haemagglutinin VP4 has been determined to a resolution of 26 Å by difference analysis of intact virions and smooth (spikeless) particles. The characteristic features of VP4 are bi-lobed head domains attached to a square-shaped body formed by two rods of density with a slight left-handed helical twist that merge with an angled rod-like domain connected to a hexameric base. The bi-lobed head and body project ~110 Å above the virion surface. The spike penetrates ~90 Å beneath the virion surface, and the rod-like domain interacts with VP7, the outer capsid protein. The broad-based anchoring domain interacts with VP7 inside the outer capsid layer as well as VP6 in the inner capsid. These structural features have implications for interactions of the virus with cell surface receptors as well as for viral morphogenesis.

## Materials and methods

### *Virus isolation, release of VP4 spikes and RNA analysis*

The SA11 strain of rotavirus was isolated from cultured MA104 cells and purified by cesium chloride density gradient centrifugation (Street *et al.*, 1982). Spikeless virions (i.e. lacking the VP4 haemagglutinin) were generated as described (Anthony *et al.*, 1991) by incubating native virions in 250 mM $NH_4OH$ at room temperature for 25 min in a buffer containing 25 mM NaCl, 1.0 mM Tris–HCl (pH 7.5) with 1.0 mM $CaCl_2$.

MA104 cells were grown in the presence of $^{32}P$, and uniformly-labeled $^{32}P$ native virions were then subjected to treatment at either pH 7 in 10 mM Tris–HCl or pH 11.2 in 1% $NH_4OH$. The radioactivity in the pellet and supernatant fractions was then measured by Cherenkov scintillation counting. SDS electrophoresis was performed using 7.5% polyacrylamide gels.

### *Cryo-electron microscopy and image processing*

Native and spikeless virions, each at a concentration of ~0.5 mg/ml, were mixed in a 1:1 ratio. Cryo-electron microscopy was performed as described (Yeager *et al.*, 1990). Grids were examined under minimal electron dose conditions at −165°C in a Philips CM12 transmission electron microscope operating at 80 kV. Two images at 0.8 and 3.0 μm defocus were recorded at 35 000 magnification from selected areas. A single micrograph was selected for processing which displayed minimal astigmatism and drift, uniform ice thickness and a field of native and spikeless virions that were not distorted, disrupted or overlapped. The micrograph was digitized at 25 μm steps, corresponding to a sampling interval of 7.14 Å at the specimen. Image processing and data displays were performed essentially as described (Yeager *et al.*, 1990). The translation (particle center) and view orientation ($\theta$, $\varphi$ and $\omega$) parameters for each virion image were iteratively refined by means of cross-correlation, and cross-common lines procedures (Crowther, 1971; Fuller, 1987; Yeager *et al.*, 1990). An initial analysis at 35 Å resolution was performed with 12 particles that displayed the best icosahedral symmetry as assessed by the cross-common lines phase residual. The origins and orientations of the initial group of four particles were refined and then fixed.

An additional group of four particles was then refined in origin and orientation. The origins and orientations of the eight particles were then fixed, and the final group of four particles was refined, yielding a 12 particle data set with self-consistent particle origins and orientations. Final refinement allowed small adjustments in all particle orientations. This initial analysis confirmed that the difference map approach would yield an interpretable VP4 density map (Yeager *et al.*, 1992). Final analysis at 26 Å resolution was carried out with 38 native and 80 spikeless particle images in which cycles of orientation refinement for all particles were alternated with cycles of origin refinement. Eigenvalue spectra provide a test for errors resulting from a non-random distribution of particle orientations (Crowther *et al.*, 1970). For both the native and spikeless particles, all eigenvalues (average of real and imaginary components) were $>1$, and 99.9% were $>10$. The completeness of the data used to compute the reconstructions was therefore clearly established. Three-dimensional reconstructions were computed by Fourier-Bessel inversion (Crowther, 1971) with icosahedral 532 symmetry imposed on the final maps (Fuller, 1987). The difference map between the native and spikeless virions was calculated by subtracting the corresponding density points in the spikeless virion map from the native virion map. Preliminary correction for contrast transfer function effects did not significantly alter the appearance of the maps or our interpretations (Cheng, 1992). Surface-shaded representations were generated using software provided by Advanced Visual Systems.

## Acknowledgements

We gratefully acknowledge the assistance of I.D.Anthony for biochemistry, M.Pique for molecular graphics and R.H.Cheng for help with contrast transfer correction calculations and in preparation of Figure 2. M.Yeager is an Established Investigator of the American Heart Association and has been supported by the National Institutes of Health (AI31535), a Grant-in-Aid from the American Heart Association, National Center (92008120), and the Gustavus and Louise Pfeiffer Research Foundation. J.A.Berriman held a New Zealand University grants committee research fellowship during this work and also received support from The Scripps Research Institute. T.S.Baker was supported by the National Institutes of Health (GM33050) and the Lucille P.Markey Charitable Trust that supports the Purdue Center for Macromolecular Structure. A.R.Bellamy was supported by the Health Research Counsel of New Zealand and the New Zealand Childrens Health Research Foundation.

## References

Adrian,M., Dubochet,J., Lepault,J. and McDowell,A.W. (1984) *Nature*, **308,** 32–36.

Anthony,I.D., Bullivant,S., Dayal,S., Bellamy,A.R. and Berriman,J.A. (1991) *J. Virol.*, **65,** 4334–4340.

Bellamy,A.R. and Both,G.W. (1990) *Adv. Virus Res.*, **38,** 1–43.

Bican,P., Cohen,J., Charpilienne,A. and Scherrer,R. (1982) *J. Virol.*, **43,** 1113–1117.

Cheng,R.H. (1992) *Proc. EMSA*, **50,** 996–997.

Clark,S.M., Roth,J.R., Clark,M.L., Barnett,B.B. and Spendlove,R.S. (1981) *J. Virol.*, **39,** 816–822.

Crowther,R.A. (1971) *Philos. Trans. R. Soc. Lond. B. Biol. Sci.*, **261,** 221–230.

Crowther,R.A., DeRosier,D.J. and Klug,A. (1970) *Proc. Roy. Soc. Lond. A.*, **317,** 319–340.

Dubochet,J., Adrian,M., Chang,J.-J., Homo,J.-C., Lepault,J., McDowall,A.W. and Schultz,P. (1988) *Q. Rev. Biophys.*, **21,** 129–228.

Esparaza,J. and Gil,F. (1978) *Virology*, **91,** 141–150.

Flores,J., Midthun,K., Hoshino,Y., Green,K., Gorziglia,M., Kapikian,A.Z. and Chanock,R.M. (1986) *J. Virol.*, **60,** 972–979.

Fukuhara,N., Yoshie,O., Kitaoka,S., Konno,T. and Ishida,N. (1987) *Arch. Virol.*, **97,** 93–99.

Fuller,S. (1987) *Cell*, **48,** 923–934.

Gorziglia,M., Larrea,C., Liprandi,F. and Esparza,J. (1985) *J. Gen. Virol.*, **66,** 1889–1900.

Gorziglia,M., Hoshino,Y., Buckler-White,A., Blumentals,I., Glass,R., Flores,J., Kapikian,A.Z. and Chanock,R.M. (1986) *Proc. Natl Acad. Sci. USA*, **83,** 7039–7043.

Graham,D.Y. and Estes,M.K., *Virology*, **101**, 432–439.

Kabcenell,A.K. and Atkinson,P.A. (1985) *J. Cell Biol.*, **101,** 1270–1280.

Kalica,A.R., Greenberg,H.B., Wyatt,R.G., Flores,J., Sereno,M.M., Kapikian,A.Z. and Chanock,R.M. (1981) *Virology*, **112,** 385–390.

Kalica,A.R., Flores,J. and Greenberg,H.B. (1983) *Virology*, **125,** 194–205.

Kaljot,K.T., Shaw,R.D., Rubin,D.H. and Greenberg,H.B. (1988) *J. Virol.*, **62,** 1136–1144.

Kapikian,A.Z. and Chanock,R.M. (1990) In Fields,B.N., Knipe,D.M., Chanock,R.M., Hirsch,M.S., Melnick,J.L., Monath,T.P. and Roizman,B. (eds), *Virology*. Raven, New York, pp. 1353–1404.

Labbé,M., Charpilienne,A., Crawford,S.E., Estes,M.K. and Cohen,J. (1991) *J. Virol.*, **65,** 2946–2952.

Liu,M., Offit,P.A. and Estes,M.K. (1988) *Virology*, **163,** 26–32.

López,S. and Arias,C.F. (1987) *Nucleic Acids Res.*, **15,** 4691.

López,S., Arias,C.F., Bell,J.R., Strauss,J.H. and Espejo,R.T. (1985) *Virology*, **144,** 11–19.

López,S., Arias,C.F., Méndez,E. and Espejo,R.T. (1986) *Virology*, **154,** 224–227.

López,S., López,I., Romero,P., Méndez,E., Soberon,X. and Arias,C.F. (1991) *J. Virol.*, **65,** 3738–3745.

Mackow,E.R., Shaw,R.D., Matsui,S.M., Vo,P.T., Benfield,D.A. and Greenberg,H.B. (1988a) *Virology*, **165,** 511–517.

Mackow,E.R., Shaw,R.D., Matsui,S.M., Vo,P.T., Dang,M.-N. and Greenberg,H.B. (1988b) *Proc. Natl Acad. Sci. USA*, **85,** 645–649.

Martin,M.L., Palmer,E.L. and Middleton,P.J. (1975) *Virology*, **68,** 146–153.

Mitchell,D.B. and Both,G.W. (1989) *Nucleic Acids Res.*, **17,** 2122.

Nishikawa,K., Taniguchi,K., Torres,A., Hoshino,Y., Green,K., Kapikian,A.Z., Chanock,R.M. and Gorziglia,M. (1988) *J. Virol.*, **62,** 4022–4026.

Offit,P.A., Blavat,G., Greenberg,H.B. and Clark,H.F. (1986) *J. Virol.*, **57,** 46–49.

Poruchynsky,M.S. and Atkinson,P.H. (1991) *J. Virol.*, **65,** 4720–4727.

Prasad,B.V.V., Wang,G.J., Clerx,J.P.M. and Chiu,W. (1988) *J. Mol. Biol.*, **199,** 269–275.

Prasad,B.V.V., Burns,J.W., Marietta,E., Estes,M.K. and Chiu,W. (1990) *Nature*, **343,** 476–479.

Shaw,A.L., Rothnagel,R., Chen,D., Ramig,R.F., Chiu,W. and Prasad,B.V.V. (1993) Cell, **74,** 693–701.

Stirzaker,S.C., Whitfeld,P.L., Christie,D.L., Bellamy,A.R. and Both,G.W. (1987) *J. Cell Biol.*, **105,** 2897–2903.

Street,J.E., Croxson,M.C., Chadderton,W.F. and Bellamy,A.R. (1982) *J. Virol.*, **43,** 369–378.

Unwin,N. (1986) *Ann. NY Acad. Sci.*, **483,** 1–4.

Wilson,I.A., Skehel,J.J. and Wiley,D.C. (1981) *Nature*, **289,** 366–373.

Yeager,M., Dryden,K.A., Olson,N.H., Greenberg,H.B. and Baker,T.S. (1990) *J. Cell Biol.*, **110,** 2133–2144.

Yeager,M., Berriman,J.A., Baker,T.S. and Bellamy,A.R. (1992) *Biophys. J.*, **61,** A7.

*Received on September 28, 1993*